Electrical detection and magnetic-field control of spin states in phosphorus-doped silicon

H. Morishita,[1] L. S. Vlasenko,[2] H. Tanaka,[3] K. Semba,[3] K. Sawano,[4] Y. Shiraki,[4] M. Eto,[1] and K. M. Itoh[1,*]
[1]*School of Fundamental Science and Technology, Keio University, 3-14-1 Hiyoshi, Kohoku-ku, Yokohama 223-8522, Japan*
[2]*A. F. Ioffe Physico-Technical Institute, Russian Academy of Sciences, 194021, St. Petersburg, Russia*
[3]*NTT Basic Research Laboratories, NTT Corporation, 3-1 Morinosato, Wakamiya, Atsugi 243-0198, Japan*
[4]*Advanced Research Laboratories, Tokyo City University, 8-15-1 Todoroki, Setagaya-ku, Tokyo 158-0082, Japan*
(Received 25 June 2009; revised manuscript received 6 October 2009; published 23 November 2009)

Electron paramagnetic resonance of ensembles of phosphorus donors in silicon has been detected electrically with externally applied magnetic fields lower than 200 G. Because the spin Hamiltonian was dominated by the contact hyperfine term rather than by the Zeeman terms at such low magnetic fields, superposition states $\alpha|\uparrow\downarrow\rangle+\beta|\downarrow\uparrow\rangle$ and $-\beta|\uparrow\downarrow\rangle+\alpha|\downarrow\uparrow\rangle$ were formed between phosphorus electron and nuclear spins, and electron paramagnetic resonance transitions between these superposition states and $|\uparrow\uparrow\rangle$ or $|\downarrow\downarrow\rangle$ states are observed clearly. A continuous change of α and β with the magnetic field was observed with a behavior fully consistent with theory of phosphorus donors in silicon.

DOI: 10.1103/PhysRevB.80.205206 PACS number(s): 76.30.−v, 03.65.Ud, 71.55.Cn, 72.20.Jv

I. INTRODUCTION

Phosphorus in silicon is attracting much attention toward realization of solid-state quantum information processors. It can be viewed as a two-qubit system having one ^{31}P nuclear spin ($I=1/2$) and one electron spin ($S=1/2$).[1–5] Coherent manipulation of its electronic states,[6–9] coherent transfer of states between electron and nuclear spins,[10] and large hyperpolarization of nuclear spins[11,12] have been demonstrated recently. Thanks to phosphorus's long spin dephasing time,[13,14] enrichment of silicon with nuclear spin-free ^{28}Si has suppressed the background isotope fluctuation significantly[15,16] to make possible the optical detection of ^{31}P nuclear spin states.[17] Because a standard electron paramagnetic resonance (EPR) measurement requires at least 10^9 spins or more, much more sensitive electrical detection methods of phosphorus EPR have been attracting attention.[6–9,19–25] The record so far reported is the detection of ~50 phosphorus spin states[23] and extensive efforts are underway worldwide to detect single phosphorus spin states.[26] All of the previous phosphorus EPR studies have been performed in the "high-magnetic-field regime," which can be defined as $B \gg 200$ G for phosphorus in silicon as we demonstrate later, and have observed two EPR allowed transitions.[6–9,11,18,23–25] The present work reports electrically detected magnetic resonance (EDMR) of phosphorus spin states in silicon which shows five of six possible transitions expected for the phosphorus donors in silicon under the low magnetic field $B \leq 200$ G.

The spin Hamiltonian of an isolated phosphorus atom placed in an externally applied magnetic field B is given by;

$$\mathcal{H}_{\mathrm{Si:P}} = g_e\mu_B B S_z - g_n\mu_n B I_z + a\boldsymbol{S}\cdot\boldsymbol{I}, \tag{1}$$

where $\boldsymbol{S}$ and $\boldsymbol{I}$ are electron and phosphorus nuclear spins, respectively. The first, second, and third terms represent the electron Zeeman, nuclear Zeeman, and contact hyperfine interaction between phosphorus electron and nuclear spins, respectively. Here $g_e\mu_B/2\pi\hbar \approx 28$ GHz/T and $g_n\mu_n/2\pi\hbar \approx 17.2$ MHz/T are given by electron and nuclear g-factors $g_e \approx 1.9985$ and $g_n \approx 2.2632$, respectively.[27,28] The hyperfine constant is $a/2\pi\hbar \approx 117.5$ MHz.[29] Eigenstates of this spin Hamiltonian are given by;

$$|1\rangle = |\uparrow\uparrow\rangle, \tag{2}$$

$$|2\rangle = \alpha|\uparrow\downarrow\rangle + \beta|\downarrow\uparrow\rangle, \tag{3}$$

$$|3\rangle = -\beta|\uparrow\downarrow\rangle + \alpha|\downarrow\uparrow\rangle, \tag{4}$$

$$|4\rangle = |\downarrow\downarrow\rangle, \tag{5}$$

where $\alpha=\cos\frac{\eta}{2}$ and $\beta=\sin\frac{\eta}{2}$. η is the angle between externally applied magnetic field direction and actual electron and nuclear spins precession axis given by $\tan\eta=\frac{a}{g_e\mu_B B-g_n\mu_n B}$.[30] A magnetic quantum number $+\frac{1}{2}$ ($-\frac{1}{2}$) is represented by $\uparrow$ ($\downarrow$) and an arrow on the left (right) in each ket represents the electron (nuclear) spin state. Figure 1(a) shows the magnetic-field dependence of the four states expected for phosphorus in silicon. At the high magnetic fields ($B \gg 200$ G), $\alpha \simeq 1$ and $\beta \simeq 0$, i.e., the four states simply become $|\uparrow\uparrow\rangle$, $|\uparrow\downarrow\rangle$, $|\downarrow\uparrow\rangle$, and $|\downarrow\downarrow\rangle$. The EPR allowed transitions in this regime are limited to two: $|\uparrow\uparrow\rangle \Leftrightarrow |\downarrow\uparrow\rangle$ and $|\uparrow\downarrow\rangle \Leftrightarrow |\downarrow\downarrow\rangle$. In the low-magnetic-field regime defined by $B \leq 200$ G, the eigenstates of $|2\rangle$ and $|3\rangle$ change continuously because η, i.e., α and β, change significantly with B as shown in Fig. 1(b). Therefore, the degree of superposition between $|\uparrow\downarrow\rangle$ and $|\downarrow\uparrow\rangle$ that determines the EPR allowed transitions also changes with B. For example, the transition $|1\rangle \Leftrightarrow |2\rangle$ at the high magnetic field corresponds to the nuclear magnetic resonance (NMR) $|\uparrow\uparrow\rangle \Leftrightarrow |\uparrow\downarrow\rangle$ and it cannot be observed as the EPR. However, the same transition becomes EPR observable at the low magnetic field because the EPR allowed component $|\uparrow\uparrow\rangle \Leftrightarrow |\downarrow\uparrow\rangle$ emerges with β. Note that transitions $|2\rangle \Leftrightarrow |3\rangle$ and $|1\rangle \Leftrightarrow |4\rangle$ are weak because they are allowed only in the second order. Nevertheless, two aspects of quantum control that cannot be realized in the high-magnetic-field regime is expected to become possible in the low-magnetic-field regime; (1) controlling the ratio of α and β to change the degree of superposi-

 ©2009 The American Physical Society

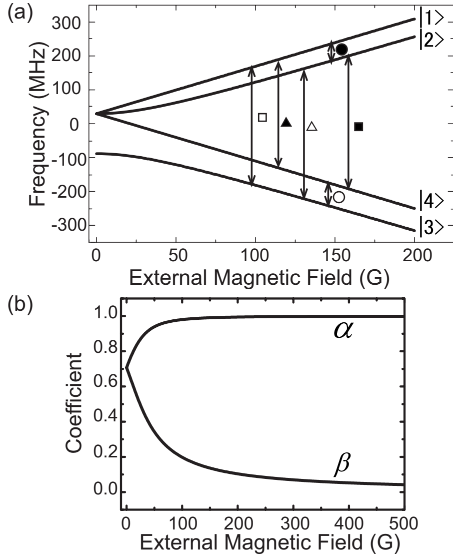

FIG. 1. (a) Externally applied magnetic-field dependence of the spin states of phosphorus in silicon defined by Eqs. (2)–(5). Six allowed transitions $|1\rangle \Leftrightarrow |3\rangle$, $|2\rangle \Leftrightarrow |4\rangle$, $|2\rangle \Leftrightarrow |3\rangle$, $|1\rangle \Leftrightarrow |4\rangle$, $|1\rangle \Leftrightarrow |2\rangle$, and $|3\rangle \Leftrightarrow |4\rangle$ are labeled by □, ■, △, ▲, ●, and ○, respectively. (b) Externally applied magnetic field dependence of α and β. $\alpha \rightarrow 1$ and $\beta \rightarrow 0$ for $B \gg 200$ G.

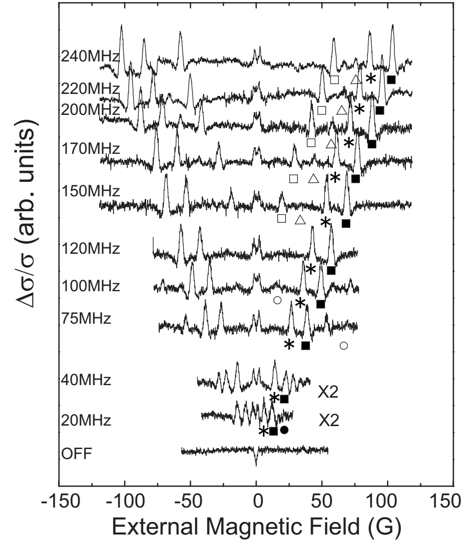

FIG. 2. EDMR signals (change in the sample photoconductivity under continuous white light illumination from a halogen lamp) vs externally applied magnetic field under irradiation of different 500 mW RF as indicated in the figure. The sample is phosphorus-doped bulk silicon single crystal ($[\mathrm{P}] \sim 10^{16}$ cm^{-3}) kept at $T=5$ K during the measurement. The peaks indicated by □ correspond to the transition $|1\rangle \Leftrightarrow |3\rangle$ labeled by the same mark in Fig. 1(a). Likewise, ■, △, ●, and ○ correspond to $|2\rangle \Leftrightarrow |4\rangle$, $|2\rangle \Leftrightarrow |3\rangle$, $|1\rangle \Leftrightarrow |2\rangle$, and $|3\rangle \Leftrightarrow |4\rangle$, respectively. Peaks labeled by * correspond predominantly to the paramagnetic resonance of the interface center for the reason discussed in the text.

tion by the magnetic field and (2) changing the population of the four states by utilizing the six transitions that are made allowed. The present work demonstrates these properties experimentally using electrical detection of phosphorus EPR and develops a quantitative theoretical model to support our observation.

II. EXPERIMENTAL

A sample was a bulk Czochralski-grown n-type silicon single crystal having phosphorus concentration $\sim 10^{16}$ cm^{-3}. It was cut into a rectangular shape of the dimension $8 \times 2 \times 1$ mm^3. Ohmic contacts were prepared at both ends of the long axis by arsenic implantation of 2×10^{15} cm^{-2} at 25 keV followed by annealing at 980 °C for 25 s and vacuum deposition of the 5-nm-thick palladium and 50-nm-thick gold layers. The sample was placed in a cryostat with optical windows. A white light from a halogen lamp placed outside of the cryostat was focused onto the sample through the optical window for steady state excitation of the electron-hole pairs to maintain the sample resistance at ~ 10 kΩ. The sample was connected with a series resistor of 10 kΩ. A constant voltage of typically 10 V was applied to the series of the sample and resistor. A coaxial cable was used to connect a radio frequency (RF) source with an irradiation coil whose opposite side was connected to a 50 Ω terminator. Externally applied magnetic field was provided by a 300 mm bore electrical magnet. Another pair coil was placed in the cryostat to modulate the externally applied magnetic field for the lock-in detection of the divider voltage corresponding to the change in the sample photoconductivity (EDMR signal).

III. RESULTS AND DISCUSSIONS

A. EDMR peak positions

Figure 2 shows the EDMR signals obtained at $T=5$ K. By changing the irradiation frequencies, six different transition peaks labeled □, ■, △, ●, ○, and * are observed clearly.

Figure 3 shows externally applied magnetic field vs RF

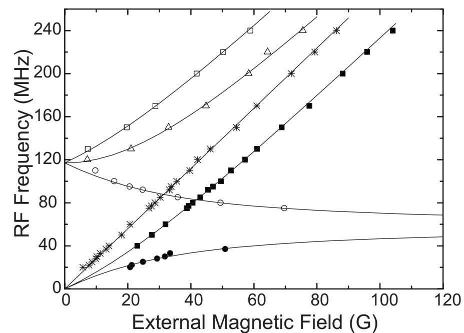

FIG. 3. A plot of irradiated frequency vs externally applied magnetic field showing positions of experimentally determined peaks represented by the same marks as in Figs. 1 and 2. The marks indicated by □, ■, △, ●, ○, and * correspond to $|1\rangle \Leftrightarrow |3\rangle$, $|2\rangle \Leftrightarrow |4\rangle$, $|2\rangle \Leftrightarrow |3\rangle$, $|1\rangle \Leftrightarrow |2\rangle$, $|3\rangle \Leftrightarrow |4\rangle$, and interface center transitions, respectively. Solid curves are rigorous theoretical calculations of resonance position of phosphorus in silicon, which show excellent agreement with experiments.

frequencies of the six observed resonance positions. Solid curves are theoretically expected results for different transitions of phosphorus in silicon using Eqs. (2)–(5) that are calculated rigorously with no fitting parameter. The excellent quantitative agreement between our experiment and theory supports the successful observation of the transitions listed in the captions of Figs. 1–3.

The transition indicated by * agrees very well with the theoretically predicted resonance positions for $|1\rangle \Leftrightarrow |4\rangle$ labeled by ▲. However, we conclude that this peak is composed predominantly by the EPR transition of the paramagnetic defects situating around the interface between bulk Si and native surface oxide SiO_2 for the following reasons. As apparent from Fig. 1(a), the transition $|1\rangle \Leftrightarrow |4\rangle$ indicated by ▲ corresponds to a typical electron Zeeman transition whose energy is approximately proportional to B. Therefore, EPR transition energies of other defects with very little hyperfine interaction, such as those of the interface spin states,[31,32] overlap with this transition. Here the EPR of the interface spin state is allowed in the first order and, therefore, expected to have strong intensity. However, the transition $|1\rangle \Leftrightarrow |4\rangle$ labeled by ▲ is allowed only in the second order and should demonstrate approximately the same intensity as the transition $|2\rangle \Leftrightarrow |3\rangle$ labeled by △ in Fig. 2. The fact that the intensity of * being much stronger than that of △ suggests that the * transition arises predominantly from the EPR transition of the interface defects that is allowed in the first order. The importance of the presence of the interface defects was confirmed by removing the surface oxide using a dilute hydrofluoric (HF) solution. The HF treatment made all of the EDMR signals nearly invisible. Leaving the sample for a few days in air to cover the sample surface with native oxide again retrieved the intensity of the all EDMR signals completely.

B. RF power and magnetic-field dependencies of the phosphorus EDMR

The fact that the presence of the surface oxide is needed to observe the EDMR signals allows us to develop a theoretical model describing the RF power and magnetic field dependencies of the EDMR signal intensity as the following. We assume that the interface defects act as spin-dependent recombination centers for electrons bound to phosphorus donors. In this sense, our model is an extension of existing two-level spin-dependent recombination model[6–9,19–21,33–40] to the four levels. The spin Hamiltonian of the system during EDMR is given by

$$\mathcal{H}_{\mathrm{EDMR}} = g_e \mu_B B_0 S_z + g_e \mu_B B_1 S_x \cos(\omega t) + a\boldsymbol{S}\cdot\boldsymbol{I}. \quad (6)$$

Here the nuclear Zeeman term is neglected because $g_n\mu_n$ is approximately 10^3 times smaller than $g_e\mu_B$ and the J coupling term ($J\boldsymbol{S}\cdot\boldsymbol{S}_1$ where $\boldsymbol{S}$ and $\boldsymbol{S}_1$ are the electron spins of the phosphorus and interface states, respectively) is also neglected assuming $a \gg J$. The second term arises from the RF irradiation and this perturbation term is defined as $\mathcal{H}'$ to calculate the transition probability W for the system described by Eq. (6) using the Fermi's golden rule,

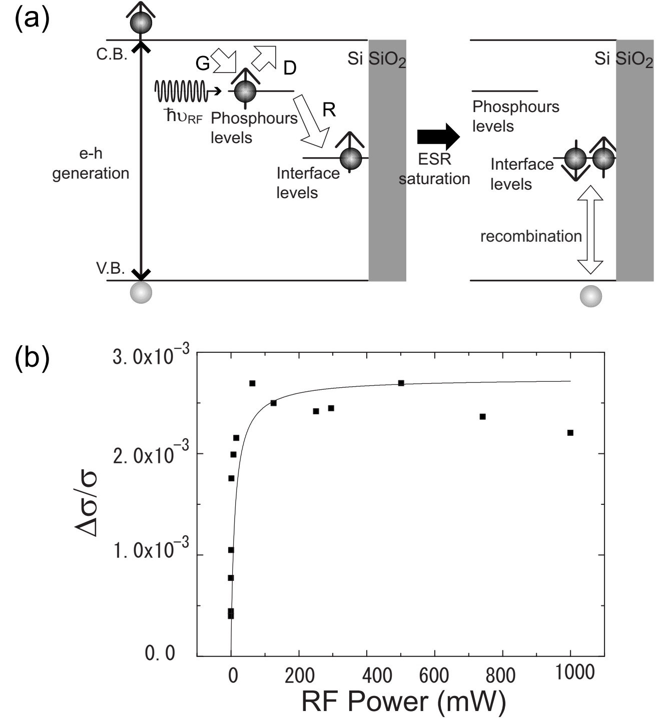

FIG. 4. (a) A schematic diagram of the EDMR mechanism. An electron at the phosphorus level undergoes spin resonance and falls to the interface level when the spin direction of phosphorus state and that of interface state form a spin singlet. Once the electron bound to phosphorus is gone, the phosphorus capturers another electron from the conduction band, leading to the change in the photoconductivity. Here the conduction electrons are captured by phosphorus at the rate G and electrons at phosphorus go back to the conduction band at the rate D or are captured by the interface states at the rate R. (b) RF power dependence of the EDMR signal for the transition $|2\rangle \Leftrightarrow |4\rangle$. The solid curve is the fitting using Eqs. (11) and (12).

$$W = \frac{2\pi}{\hbar} |\langle f|\mathcal{H}'|i\rangle|^2 \delta(E_f - E_i - \hbar\nu). \quad (7)$$

The electron-hole recombination via interface states takes place only when $\boldsymbol{S}$ and $\boldsymbol{S}_1$ form a spin singlet and does not occur when they form a spin triplet to establish a "spin blockade."[41]

Other important essences of our model are described in the caption of Fig. 4(a). Let us consider $|i\rangle$ where $i=1, 2, 3$, or 4 is one of the four phosphorus spin states as defined by Eqs. (2)–(5) and $|\sigma\rangle$ where $\sigma=\uparrow$ or $\downarrow$ corresponds to spin up or down of the interface state, respectively. Using G, D, and R defined in Fig. 4(a), we obtain the rate equation

$$\frac{d}{dt} N_{i\sigma} = G\left(N - \sum_{j\sigma'} N_{j\sigma'}\right) - (D + R_{i\sigma}) N_{i\sigma}, \quad (8)$$

where N is the total number of electron pairs and $N_{i\sigma}$ is the number of electron pairs in spin states i and σ. The recombination rates $R_{i\sigma}$ that have been obtained using the method described in Ref. 42 are listed in Table I. The pairs with (i,σ) with $R_{i\sigma}=0$ correspond to the spin blockade. Now we con-

TABLE I. Recombination rate of each transition between phosphorus and interface spin states.[42]

$R_{i\sigma}$	Phosphorus	Interface	Recombination rate
$R_{1\uparrow}$	$\|\uparrow\uparrow\rangle$	$\|\uparrow\rangle$	0
$R_{1\downarrow}$	$\|\uparrow\uparrow\rangle$	$\|\downarrow\rangle$	$\frac{1}{2}R$
$R_{2\uparrow}$	$\alpha\|\uparrow\downarrow\rangle+\beta\|\downarrow\uparrow\rangle$	$\|\uparrow\rangle$	$\frac{1}{2}\beta^2R$
$R_{2\downarrow}$	$\alpha\|\uparrow\downarrow\rangle+\beta\|\downarrow\uparrow\rangle$	$\|\downarrow\rangle$	$\frac{1}{2}\alpha^2R$
$R_{3\uparrow}$	$-\beta\|\uparrow\downarrow\rangle+\alpha\|\downarrow\uparrow\rangle$	$\|\uparrow\rangle$	$\frac{1}{2}\alpha^2R$
$R_{3\downarrow}$	$-\beta\|\uparrow\downarrow\rangle+\alpha\|\downarrow\uparrow\rangle$	$\|\downarrow\rangle$	$\frac{1}{2}\beta^2R$
$R_{4\uparrow}$	$\|\downarrow\downarrow\rangle$	$\|\uparrow\rangle$	$\frac{1}{2}R$
$R_{4\downarrow}$	$\|\downarrow\downarrow\rangle$	$\|\downarrow\rangle$	0

sider a representing example where the irradiated RF is in resonance with the $|2\rangle \Leftrightarrow |4\rangle$ transition. In this case;

$$\frac{d}{dt}N_{2\sigma} = G\left(N - \sum_{j\sigma'} N_{j\sigma'}\right) - (D + R_{2\sigma})N_{2\sigma} - W(N_{2\sigma} - N_{4\sigma}),$$

$$\frac{d}{dt}N_{4\sigma} = G\left(N - \sum_{j\sigma'} N_{j\sigma'}\right) - (D + R_{4\sigma})N_{4\sigma} + W(N_{2\sigma} - N_{4\sigma}), \tag{9}$$

where $W \propto (g_e\mu_B B_1/2)^2\alpha^2$ is the transition probability that is proportional to the RF irradiation power around the origin.[43] This partly lifts the spin blockade and promotes the recombination. The steady state solution for the number of electron recombining $I(W)$ becomes;

$$I(W) = \frac{NG}{1 + G\left[\sum_{i\sigma} \frac{1}{D + R_{i\sigma}} - WX(W)\right]} \times \left[\sum_{i\sigma} \frac{R_{i\sigma}}{D + R_{i\sigma}} + WDX(W)\right], \tag{10}$$

$$X(W) = \sum_{\sigma} \frac{1}{(D + R_{2\sigma})(D + R_{4\sigma})} \times \frac{(R_{2\sigma} - R_{4\sigma})^2}{(2D + R_{2\sigma} + R_{4\sigma})W + (D + R_{2\sigma})(D + R_{4\sigma})}. \tag{11}$$

Then the EDMR signal intensity S_{EDMR} is obtained as;

$$S_{EDMR} = I(W) - I(0) = NG\frac{D + 8G}{1 + G\sum_{i\sigma}\frac{1}{D + R_{i\sigma}}} \times \frac{WX(W)}{1 + G\left[\sum_{i\sigma}\frac{1}{D + R_{i\sigma}} - WX(W)\right]}. \tag{12}$$

This result shows that the signal intensity is proportional to the irradiated RF power and, therefore, to W around the origin. This corresponds to our experimental observation shown in Fig. 4(b) when $\Delta\sigma/\sigma$ is defined as $S_{EDMR}/I(0)$. A solid curve shown in the figure is the successful fitting by Eqs. (11) and (12) using N, G, D, and R as fitting parameters. A set of appropriate values we found are $N = 6.4 \times 10^5$ cm^{-3}, $G = 5.0 \times 10^{-9}$ sec^{-1}, $D = 2.3 \times 10^1$ sec^{-1}, and $R = 1.7 \times 10^1$ sec^{-1}.

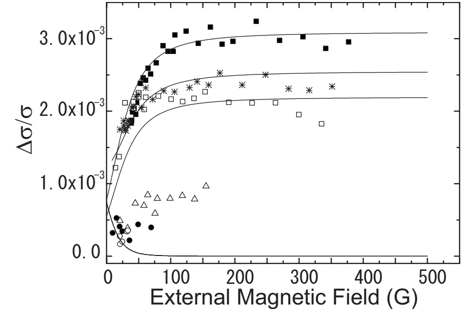

FIG. 5. EDMR intensity vs externally applied magnetic field. Experimentally determined positions are represented by the same marks in as Fig. 2. The peaks indicated by □, ■ △, ●, ○, and * correspond to $|1\rangle \Leftrightarrow |3\rangle$, $|2\rangle \Leftrightarrow |4\rangle$, $|2\rangle \Leftrightarrow |3\rangle$, $|1\rangle \Leftrightarrow |2\rangle$, $|3\rangle \Leftrightarrow |4\rangle$, and interface center transitions, respectively. Solid curves are fittings for allowed transitions □, ■, ●, and ○ using Eqs. (12) and (13) with $WX(W)$ as described in the text. The fits for ● and ○ overlap completely. The interface center transition * is fitted with Eqs. (12) and (15).

Finally, we show in Fig. 5 the magnetic field dependence of the EDMR signal intensity. We used the RF power of 500 mW, which was large enough to saturate the signal as shown in Fig. 4(b). Here $W \gg D, R$. Now the two $WX(W)$'s in Eq. (11) are replaced by a constant;

$$WX(W) \to \sum_{\sigma} \frac{1}{(D + R_{2\sigma})(D + R_{4\sigma})} \cdot \frac{(R_{2\sigma} - R_{4\sigma})^2}{2D + R_{2\sigma} + R_{4\sigma}}. \tag{13}$$

Such relations with appropriate $R_{i\sigma}$ have been used to fit representative experimental results shown in Fig. 5. Note that our model is not applicable to second order allowed transitions such as $|2\rangle \Leftrightarrow |3\rangle$ and $|1\rangle \Leftrightarrow |4\rangle$. From the fitting of the first order allowed $|2\rangle \Leftrightarrow |4\rangle$ transition, we obtain a set of appropriate values $N = 1.0 \times 10^4$ cm^{-3}, $G = 6.7 \times 10^{-6}$ sec^{-1}, $D = 2.9 \times 10^1$ sec^{-1}, and $R = 7.0 \times 10^{-1}$ sec^{-1}. Note that the magnetic field dependence of α and β employed here is same as the one shown in Fig. 1(b). Therefore, the excellent agreement between our experiment and model shows that the coefficients of superposition can be controlled by the choice of B and reach the maximally entangled states $1/\sqrt{2}(|\uparrow\downarrow\rangle + |\downarrow\uparrow\rangle)$ in the limit of $B = 0$ as expected.[44]

Similarly, we can derive a relation for the interface center EDMR, since the rotation of the interface electron spin $\boldsymbol{S}_1$ also lifts the spin blockade and enhances the recombination. We consider again a rate equation using N, G, D, and R to obtain the same S_{EDMR} as Eq. (12) but different $X(W)$ from the phosphorus resonance case:[45]

$$X(W) = \sum_{i=1}^{4} \frac{1}{(D+R_{i\uparrow})(D+R_{i\downarrow})} \times \frac{(R_{i\uparrow}-R_{i\downarrow})^2}{(2D+R_{i\uparrow}+R_{i\downarrow})W+(D+R_{i\uparrow})(D+R_{i\downarrow})}. \quad (14)$$

When the signal intensity is saturated, $WX(W)$ is given by;

$$WX(W) \to \sum_{i=1}^{4} \frac{1}{(D+R_{i\uparrow})(D+R_{i\downarrow})} \cdot \frac{(R_{i\uparrow}-R_{i\downarrow})^2}{2D+R_{i\uparrow}+R_{i\downarrow}}. \quad (15)$$

This result has been used to fit the behavior of the interface center peak (*) in Fig. 5. A set of appropriate values we found are $N=8\times10^3$ cm^{-3}, $G=2.0\times10^{-5}$ sec^{-1}, $D=3.6\times10^1$ sec^{-1}, and $R=3.9\times10^{-1}$ sec^{-1}. Here the values of N, D, and R are approximately the same as the ones obtained for phosphorus but the value of G is different.

A significance of the results shown in Fig. 5 is that the intensity of transitions changes below 200 G in accordance with theory. The standard EPR allows for observation of only $|1\rangle \Leftrightarrow |3\rangle$ and $|2\rangle \Leftrightarrow |4\rangle$ because $\beta=0$ in the high magnetic fields. However, the value of β increases with decreasing the magnetic field, especially for the magnetic fields below 200 G, and approaches $1/\sqrt{2}$ as $B\to 0$. Naturally, the intensity of $|1\rangle \Leftrightarrow |3\rangle$ and $|2\rangle \Leftrightarrow |4\rangle$ decreases because the components of the EPR allowed $|\uparrow\uparrow\rangle \Leftrightarrow |\downarrow\uparrow\rangle$ and $|\uparrow\downarrow\rangle \Leftrightarrow |\downarrow\downarrow\rangle$ diminish. For the same reason transitions such as $|1\rangle \Leftrightarrow |2\rangle$ and $|3\rangle \Leftrightarrow |4\rangle$ appear only when $B \leq 200$ G. This observation leads us to conclude that it is possible to form the superposition states between electron and nuclear spins of phosphorus in the regime of the low magnetic field $B \leq 200$ G. Their superposition coefficients α and β can be controlled simply by selecting an appropriate magnetic field.

IV. CONCLUSION

Electron paramagnetic resonance spectroscopy of an ensemble of phosphorus donors in silicon has been performed successfully to map out the behavior of phosphorus spin states at the magnetic field lower than 200 G. Formation of the superposition states $\alpha|\uparrow\downarrow\rangle+\beta|\downarrow\uparrow\rangle$ and $-\beta|\uparrow\downarrow\rangle+\alpha|\downarrow\uparrow\rangle$ has been confirmed with the values of α and β changing continuously with the magnetic field in accordance with theory of phosphorus in silicon. Dependencies of the EDMR signal intensity on the RF power and magnetic field have been described successfully by a model assuming a spin-dependent recombination of phosphorus electrons via defects situating around the oxide/silicon interface.

ACKNOWLEDGMENTS

We thank Martin Brandt for fruitful discussion. This work was supported in part by a Grant-in-Aid for Scientific Research by MEXT Specially Promoted Research No. 18001002, in part by Special Coordination Funds for Promoting Science and Technology, in part by the JST-DFG Strategic Cooperative Program on Nanoelectronics, in part by the Strategic Information and Communications R&D Promotion Program (SCOPE) from the Ministry of Internal Affairs and Communications of Japan, and in part by a Grant-in-Aid for the Global Center of Excellence at Keio University.

---

*kitoh@appi.keio.ac.jp

[1] B. E. Kane, Nature (London) **393**, 133 (1998).
[2] B. E. Kane, Fortschr. Phys. **48**, 1023 (2000).
[3] K. M. Itoh, Solid State Commun. **133**, 747 (2005).
[4] M. Sarovar, K. C. Young, T. Schenkel, and K. B. Whaley, Phys. Rev. B **78**, 245302 (2008).
[5] C. Boehme and K. Lips, Phys. Status Solidi **233**, 427 (2002) b.
[6] A. R. Stegner, C. Boehme, H. Huebl, M. Stutzmann, K. Lips, and M. S. Brandt, Nat. Phys. **2**, 835 (2006).
[7] H. Huebl, F. Hoehne, B. Grolik, A. R. Stegner, M. Stutzmann, and M. S. Brandt, Phys. Rev. Lett. **100**, 177602 (2008).
[8] G. W. Morley, D. R. McCamey, H. A. Seipel, L.-C. Brunel, J. van Tol, and C. Boehme, Phys. Rev. Lett. **101**, 207602 (2008).
[9] F. Hoehne, H. Huebl, B. Galler, M. Stutzmann, and M. S. Brandt, arXiv:0908.3612 (unpublished).
[10] J. J. L. Morton, A. M. Tyryshkin, R. M. Brown, S. Shankar, B. W. Lovett, A. Ardavan, T. Schenkel, E. E. Haller, J. W. Ager, and S. A. Lyon, Nature (London) **455**, 1085 (2008).
[11] D. R. McCamey, J. van Tol, G. W. Morley, and C. Boehme, Phys. Rev. Lett. **102**, 027601 (2009).
[12] A. Yang, M. Steger, T. Sekiguchi, M. L. W. Thewalt, T. D. Ladd, K. M. Itoh, H. Riemann, N. V. Abrosimov, P. Becker, and H.-J. Pohl, Phys. Rev. Lett. **102**, 257401 (2009).
[13] A. M. Tyryshkin, J. J. L. Morton, S. C. Benjamin, A. Ardavan, G. A. D. Briggs, J. W. Ager, and S. A. Lyon, J. Phys.: Condens. Matter **18**, S783 (2006).
[14] E. Abe, K. M. Itoh, J. Isoya, and S. Yamasaki, Phys. Rev. B **70**, 033204 (2004).
[15] K. M. Itoh, J. Kato, F. Uemura, A. K. Kaliteyevskii, O. N. Godisov, G. G. Devyatych, A. D. Bulanov, A. V. Gusev, I. D. Kovalev, P. G. Sennikov, H.-J. Pohl, N. V. Abrosimov, and H. Riemann, Jpn. J. Appl. Phys. **42**, 6248 (2003).
[16] K. Takyu, K. M. Itoh, K. Oka, N. Saito, and V. I. Ozhogin, Jpn. J. Appl. Phys. **38**, L1493 (1999).
[17] A. Yang, M. Steger, D. Karaiskaj, M. L. W. Thewalt, M. Cardona, K. M. Itoh, H. Riemann, N. V. Abrosimov, M. F. Churbanov, A. V. Gusev, A. D. Bulanov, A. K. Kaliteevskii, O. N. Godisov, P. Becker, H.-J. Pohl, J. W. Ager III, and E. E. Haller, Phys. Rev. Lett. **97**, 227401 (2006).
[18] J. Schmidt and I. Solomon, Compt. Rend. **263**, 169 (1966).
[19] B. Stich, S. Greulich-Weber, and J.-M. Speath, J. Appl. Phys. **77**, 1546 (1995).
[20] S. Greulich-Weber, B. Stich, and J.-M. Spaeth, Mater. Sci. Forum **196-201**, 1509 (1995).
[21] J.-M. Spaeth and H. Overhof, *Point Defects in Semiconductors and Insulators* (Springer, New York, 2002), Chap. 7.

[22] B. Stich, S. Greulich-Weber, and J.-M. Speath, Appl. Phys. Lett. **68**, 1102 (1996).
[23] D. R. McCamey, H. Huebl, M. S. Brandt, W. D. Hutchison, J. C. McCallum, R. G. Clark, and A. R. Hamilton, Appl. Phys. Lett. **89**, 182115 (2006).
[24] D. R. McCamey, G. W. Morley, H. A. Seipel, L.-C. Brunel, J. van Tol, and C. Boehme, Phys. Rev. B **78**, 045303 (2008).
[25] A. Honig and M. Moroz, Rev. Sci. Instrum. **49**, 183 (1978).
[26] K. Y. Tan, K. W. Chan, M. Möttönen, A. Morello, C. Yang, J. van Donkelaar, A. Alves, J. M. Pirkkalainen, D. N. Jamieson, R. G. Clark, and A. S. Dzurak, arXiv:0905.4358 (unpublished).
[27] C. F. Young, E. H. Poindexter, G. J. Gerardi, W. L. Warren, and D. J. Keeble, Phys. Rev. B **55**, 16245 (1997).
[28] J. E. Mack, Rev. Mod. Phys. **22**, 64 (1950).
[29] G. Feher, Phys. Rev. **114**, 1219 (1959).
[30] A. Schweiger and G. Jeschke, *Principles of Pulse Electron Paramagnetic Resonance* (Oxford, 2001), Chap. 3, Sec. 3.5, pp.58–62.
[31] D. J. Lépine, Phys. Rev. B **6**, 436 (1972).
[32] J. L. Cantin and H. J. von Bardeleben, J. Non-Cryst. Solids **303**, 175 (2002).
[33] R. M. White and J. F. Gouyet, Phys. Rev. B **16**, 3596 (1977).
[34] D. Kaplan, I. Solomon, and N. F. Mott, J. Phys. (France) Lett. **39**, 51 (1978).
[35] R. Haberkorn and W. Dietz, Solid State Commun. **35**, 505 (1980).
[36] V. S. L'vov, L. S. Mima, and O. V. Tretyak, Sov. Phys. JETP **56**, 897 (1982).
[37] L. S. Vlasenko, Yu. V. Martynov, T. Gregorkiewicz, and C. A. J. Ammerlaan, Phys. Rev. B **52**, 1144 (1995).
[38] A. V. Barabanov, O. V. Tretiak, and V. A. L'vov, Phys. Rev. B **54**, 2571 (1996).
[39] A. V. Barabanov, V. A. Lvov, and O. V. Tretyak, Phys. Status Solidi **207**, 419 (1998) b.
[40] A. Gliesche, C. Michel, V. Rajevac, K. Lips, S. D. Baranovskii, F. Gebhard, and C. Boehme, Phys. Rev. B **77**, 245206 (2008).
[41] A similar phenomenon was observed in transport through double quantum dots in K. Ono *et al.*, Science **297**, 1313 (2002).
[42] R is the transition rate of an electron from phosphorus to the interface levels when $\boldsymbol{S}$ and $\boldsymbol{S}_1$ form a spin singlet. The transition rate $\propto \exp[-r(a_B^{*-1}+a_i^{-1})]$, where r is the distance between a phosphorus and an interface state and $a_B^*(a_i)$ is the effective Bohr radius of phosphorus (interface) state. It is averaged with the weight of $P(r)=-\frac{d}{dr}\exp(-4\pi r^3 n_D/3)$, where n_D is the donor concentration.
[43] On the other hand, the transition probabilities of $|1\rangle \Leftrightarrow |2\rangle$, $|1\rangle \Leftrightarrow |3\rangle$, and $|3\rangle \Leftrightarrow |4\rangle$ are proportional to β^2, α^2, and β^2, respectively.
[44] C. H. Bennett, H. J. Bernstein, S. Popescu, and B. Schumacher, Phys. Rev. A **53**, 2046 (1996).
[45] The rate equations given by $\frac{d}{dt}N_{i\sigma}=G(N-\Sigma_{j\sigma'}N_{j\sigma'})-(W+D+R_{i\sigma})N_{i\sigma}+WN_{i\bar{\sigma}}$, where $\bar{\sigma}=\uparrow(\downarrow)$ for $\sigma=\downarrow(\uparrow)$ and $W \propto (g\mu_B B/2)^2$.